

Choosing the Most Suitable Working Fluid for a CTEC

Aliet Achkienasi ¹, Rodolfo Silva ¹, Edgar Mendoza ^{1,*} and Luis D. Luna ²

¹ Instituto de Ingeniería, Universidad Nacional Autónoma de México, Mexico City 04510, Mexico; aachkienasia@iingen.unam.mx (A.A.); rsilvac@iingen.unam.mx (R.S.)

² Dipartimento di Ingegneria, Università Degli Studi Della Campania Luigi Vanvitelli, Viale Abramo Lincoln n. 5, 81100 Caserta, Italy; luisdaniel.lunaaguilar@unicampania.it

* Correspondence: emendozab@iingen.unam.mx

Abstract: This study aims to explore additional fluids beneficial for coastal thermal energy converter (CTEC) operation. Ammonia's thermodynamic properties, characterized by higher condensation temperatures and pressures, demand significantly elevated operating pressures, resulting in a substantial energy load for efficient operation. Thus, exploring alternatives such as R134a becomes crucial, particularly considering its potential as a better working fluid for power generation in a Rankine cycle. The research methodology involves employing computational fluid dynamics (CFD) simulations alongside experimental investigations to examine the performance of an axial turbine concept under different working fluids. The results obtained indicate that R134a is the most appropriate working fluid for an axial turbine within a CTEC, outperforming ammonia, thereby implying significantly better operational efficiency.

Keywords: coastal thermal energy conversion; CTEC experiments; working fluid; CFD numerical modelling for CTEC

1. Introduction

Electricity is produced around the world from non-renewable sources, such as fossil and nuclear fuels, and renewable sources, such as solar, hydraulic, biomass, wind, and marine energy. Although the latter sources are being developed, most electricity still comes from thermoelectric plants [1].

Almost all electricity-generating plants burn fossil fuels to produce water vapor in a boiler. High-pressure steam drives a turbine and produces electricity. After the steam passes through the turbine, it is taken to a cooling tower, where it is condensed to be used again in the boiler, a process that is repeated indefinitely [2].

The resulting thermal waste is usually dumped into the sea. The idea of generating energy from this has led to the development of coastal thermal energy converters (CTECs) [3]. A CTEC is similar in principle to the more well-known ocean thermal energy conversion devices (OTECs), but would use the thermal gradient from the cooling process of the condenser of a thermoelectric plant with cold water from greater depths to generate energy via a closed Rankine cycle. CTECs would obviously be located on the coast, near to a thermoelectric power plant [4]. Currently, there are no OTEC or CTEC plants operating commercially, but they have been widely studied in recent years.

Liu et al. [5] provided a comprehensive review of closed thermodynamic cycles in ocean thermal energy conversion (OTEC) systems, detailing both pure and mixed working fluids and elucidating their impact on cycle efficiency.

Among the studies that have been carried out on OTEC systems are:

- Mini OTEC-CC, 50 kW (1979), a closed-cycle system, was operated on a US Navy barge 2 km off the coast of Keahole Point, Hawaii. This plant operated for three months in 1979, using ammonia as a working fluid, generating 50 kW of gross power and net power of 10–17 kW [5].



Citation: Achkienasi, A.; Silva, R.; Mendoza, E.; Luna, L.D. Choosing the Most Suitable Working Fluid for a CTEC. *Energies* **2024**, *17*, 2181. <https://doi.org/10.3390/en17092181>

Academic Editor: Adrian Ilinca

Received: 2 April 2024

Revised: 19 April 2024

Accepted: 29 April 2024

Published: 2 May 2024



Copyright: © 2024 by the authors. Licensee MDPI, Basel, Switzerland. This article is an open access article distributed under the terms and conditions of the Creative Commons Attribution (CC BY) license (<https://creativecommons.org/licenses/by/4.0/>).

- OTEC-1 MW (1980) was deployed on a US Navy tanker anchored off Kawaihae, on the coast of Kona, Hawaii. It was used to test heat exchangers and other components of a closed cycle plant, and for research into environmental effects on the ocean [6].
- OTEC-CC 100 kW (1981), the first land-based system, was installed in the Republic of Nauru in Micronesia, by Toshiba, TEPCO, and Tokyo Electric Power Services [7].
- A 210 kW OC-OTEC experimental plant was installed on land in Hawaii, and operated from 1993 until 1998 as a test bank for future modifications and improvements in the OTEC process, producing electricity and desalinated water [8].
- A 1 MW floating OTEC plant, approximately 60 km southeast of the Port of Tuticorin, India, was installed by Saga University, Japan and NIOT of India in 2000, using ammonia as the working fluid [9].
- A 20 kW closed loop was designed in 2012 by KRISO (Korea Research Institute of Ships and Ocean Engineering), together with KIOST (Korea Institute of Ocean Science and Technology). It served as a prototype for a later plant of 1 [MW], installed in 2013. The working fluid was the refrigerant R-32 [10].
- A 10 MW plant was developed by Lockheed Martin and the Beijing Based Reignwood Group. It was installed on the south coast of China in 2013 [10].
- A 100 kW plant was installed in Hawaii in 2015, working in a closed cycle, with ammonia as the working fluid. It can supply electricity to 120 houses [11].

While Zhang et al. [12] focused on ammonia and employed a radial turbine, our study extends this research by exploring the effectiveness of R134a with an axial turbine, broadening the understanding of viable working fluids in OTEC technology.

In almost all of the aforementioned studies, the working fluid used was ammonia. However, there are no data for other working fluids for any comparison studies. To improve efficiency and make the process more environmentally sustainable, using other working fluids, especially those with low boiling points, may be feasible.

Qingfen Ma et al. [13] explored an OTEC-ORC plant employing a non-azeotropic mixture of hydrofluoroolefins (HFOs), showcasing superior performance over NH_3 . Furthermore, the study included the design and simulation of a gas turbine, demonstrating impressive output power and efficiency, confirming the potential of the ORC with the HFO mixture as an alternative to NH_3 . Additionally, Min-Hsiung Yang et al. [14] investigate R717 blends, integrating the environmentally friendly refrigerants R32 and R1234YF, showing significant enhancements in net power output and economic efficiency.

The primary objective of this work is to select the most suitable working fluid for the operation of a CTEC, using various methodologies, such as Cerezo et al., experimentation in the laboratory, and CFD modeling. Steam, R134-a, and ammonia are evaluated, with a focus on heat transfer characteristics, and the overall operational behavior of an axial turbine.

The significant achievements of this research are in the development of a laboratory model, and the experimentation conducted with steam. Subsequently, through mathematical modeling, we identified the most suitable working fluid between R134a and ammonia for utilization in energy production through OTEC.

In recent years, computational fluid dynamics (CFD) technology has significantly advanced our understanding of fluid flow phenomena. Research by Qing Yan and Gaoan Zheng [15] has contributed to this field, particularly in investigating two-phase slug flow in pipelines. Yan focused on mixed-transport pipelines, using a VOF-based model to analyze slug flow formation. Meanwhile, Zheng [16] explored slug flow in marine pipelines, employing a VOF-PLIC-based model to uncover periodic flow characteristics and the impact of gas-phase velocity changes. These studies have provided valuable insights for optimizing pipeline designs and mitigating vibrations.

Raimunda da Silva and colleagues [17] introduced a preliminary design and optimization methodology tailored for radial turbines within organic Rankine cycle (ORC) applications. Their study employed an optimization algorithm to enhance efficiency, yielding notable results, with 82.4% efficiency achieved in a final design employing R245fa. In a complementary effort, Yu et al. [18] presented an innovative methodology focused on

coupling ORC systems with radial turbine rotors to maximize waste heat recovery. Their approach yielded impressive results, with a net power output of 393.06 kW and a significant 7.5% increase achieved through optimization. Additionally, Obert and collaborators [19] examined the complexities of ORC turbine performance through CFD simulations, particularly emphasizing the non-ideal behavior of hexamethyldisiloxane (MM). Their study meticulously assessed stator/rotor flow interaction effects on blade performance and flow structure, shedding light on critical factors influencing turbine efficiency and operation. Together, these studies contributed to advancing our understanding and optimization of ORC technology and the CFD approach.

Regarding heat exchangers, J.S. Jayakumar's study [20] highlighted the inadequacy of constant boundary conditions and advocates for considering conjugate heat transfer and temperature-dependent properties on helically coiled heat exchangers. Additionally, it compared experimental results with CFD calculations, and developed a correlation based on the experimental data to calculate the inner heat transfer coefficient of the helical coil.

While our study did not explore heat transfer phenomena associated with phase changes, we prioritized other simulation aspects that aligned with our research's specific objectives and scope. Nevertheless, we acknowledge the significance of integrating heat transfer considerations when they are pertinent to the study's objectives or practical applications.

Deng et al. [21] proposed integrating seawater desalination with energy utilization systems to tackle China's energy and freshwater shortages. They presented three feasible integration methods: combined cooling, heating, and power systems, power plants, and solar thermal utilization systems. This integration offered a promising solution to improve freshwater supply and optimize low-temperature thermal energy utilization in coastal regions.

The current research is presented here as follows: Section 2 shows the methodology used and outlines the criteria guiding the selection of working fluids for subsequent analysis. Details on the construction process of the laboratory model and the presentation of theoretical Rankine cycles for the chosen working fluids are also included in Section 2. Section 3 presents and discusses the results obtained from the laboratory model, it focuses on the crucial aspects of mesh and convergence in the simulation process and presents the numerical model results for steam and the working fluids selected, respectively. The research concludes in Section 4, with the key findings and their implications.

2. Materials and Methods

The methodology used in this paper is shown in Figure 1.

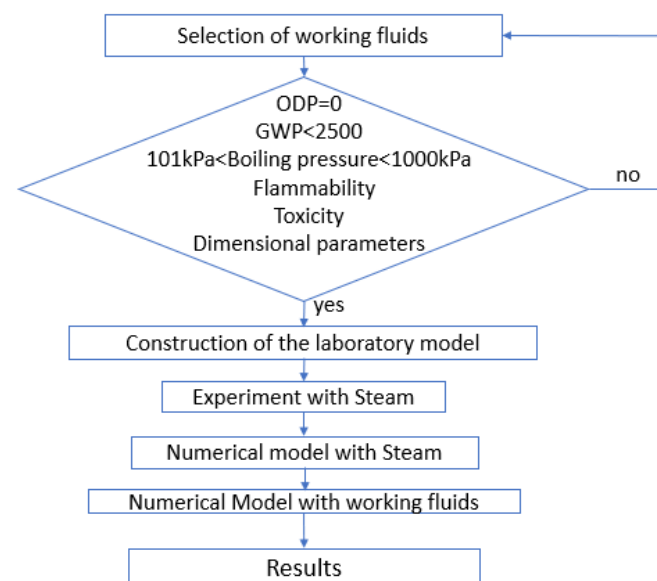


Figure 1. Overview of the methodology presented.

2.1. Subsection

The selection of the working fluid is crucial for maximizing OTEC plant efficiency, as fluid thermodynamics directly impact component size and overall system cost [22].

To select the most suitable working fluid for use in the experiment, the methodology of Cerezo et al. (2020) was used, where the following factors must be considered [23]:

1. Ozone layer destruction potential (ODP)
2. Heating power, GWP (Global Warming Potential)
3. Boiling pressure at 15.56 °C
4. Flammability
5. Toxicity
6. Parameters for sizing the turbine and heat exchanger.
7. Cost of the working fluid

Based on these criteria, those fluids that had either of the following characteristics were dismissed: (1) ODP > 0; (2) GWP > 2500 (according to European legislation, it is the same limit used for fixed refrigeration systems) [24,25].

The sizing parameters (point six) use a factor, B , with the units kPa M kJ/kg. This is inversely proportional to the mass flow, which determines the lowest mass flow for the operation of the plant [4].

$$B = p_v \times \Delta H_{lg} \times M \quad (1)$$

where:

p_v is the saturation pressure at 1 atm in kPa

ΔH_{lg} is the enthalpy change due to phase change (kJ/kg)

M is the molecular weight

A maximum value of B corresponds to the minimum volume required for the construction of the turbine, piping, and associated valves, thus reducing the blades and suction pipe cross-section. For the sizing of the exchanges, the aim is to reduce their area, which is obtained from:

$$a = \frac{\dot{Q}}{U_0 \Delta T_m} \quad (2)$$

where:

\dot{Q} is the heat flux (W)

U_0 is the global coefficient of the exchanger (W/m² °C)

a is the exchanger area (m²)

The convection heat transfer coefficient h can be expressed by the relationship (3):

$$h = \left(\frac{k^3 \times \rho_l^2 \times \Delta H_{lg}}{\theta \times \mu_l \times \Delta T} \right)^{1/4} \quad (3)$$

where:

k is the thermal conductivity (W/mK)

ρ_l is the density (kg/m³)

θ is the pipe diameter (m)

μ_l is the dynamic viscosity (Pa s)

For a given temperature and pipe diameter:

$$h = constant \left(\frac{k^3 \rho^2 H_{lg}}{\mu} \right)^{1/4} = constant * \varphi \quad (4)$$

$$\varphi = \left(\frac{k^3 \times \rho^2 \times H_{lg}}{\mu} \right)^{1/4} \quad (5)$$

The minimum heat exchanger area corresponds to the maximum value of φ .

Once the physical and safety properties of the working fluids were obtained, the linear weighting method was used for decision-making, assigning weights over 100% to the evaluation criteria, in accordance with their importance.

The overall rating of each working fluid was calculated by adding the products of the scores obtained for each criterion according to their assigned weight.

Since the criteria were given on different scales, they could not be summed directly, so a prior normalization process was required.

2.2. Laboratory Model

The next phase was to build a laboratory model that used steam as the working fluid. This decision was made because working fluids with a low boiling point require very high pressures to maintain their fluid state.

The construction of the experimental model was carried out in three stages:

Stage 1. Selection and tests of the evaporator: an electric tank water heater was the most suitable option to produce steam by regulating the incoming water flow, ensuring that only the necessary amount of water entered to match the capacity for evaporation.

A 127 volt water heater, manufactured by Rheem, with a capacity of 9 L was chosen. The thermostat, which normally prevented the temperature from rising above 60 °C, was removed for the experiment.

The pipes and connections were copper. The outlet and inlet of the heater were of 1/2" diameter. To increase the pressure within the system solely through evaporation in the boiler, the diameter of the pipes in the rest of the system was reduced to 3/8", the smallest diameter available on the market.

It was seen that the evaporation capacity of the model was 40 mL/min, and that optimal operation occurred when 6 L of water was inside it. Once connected, it took 35–40 min to reach and maintain a constant steam flow of around 40 mL/min.

To achieve the required steam flow to drive the turbine, the pressure within the system had to be increased, so a ball valve and a Instrutec manometer (with a range of 3 psi) were installed.

Stage 2. Turbine design, 3D printing and testing: The turbine was designed in AutoCAD 2023, being similar to a Pelton turbine with tangential flow. The 3D printing of the turbine was performed on a Stratasys Fortus 450 mc printer. After several material resistance tests, it was decided to use ASA from Stratasys. In Figure 2, the turbine used is depicted. The casing (A) was coated with epoxy paste and two layers of marine-grade primer to prevent leaks. On the cover (B), the turbine blades were assembled, along with the motor acting as an electrical generator (C), which was equipped with a small LED that illuminated during the experimentation.

The porosity of the material was greater than we expected, so water droplets seeped through the casing. To reduce this, the turbine and the internal parts of the casing and cover were coated with an epoxy paste with steel load, designed for automotive use. To improve the finish, two coats of Rust-Oleum spray primer were also applied.

The RF-500TB-14415 motor used as a generator was made by Mabuchi Motor. Its operating parameters are found in Table 1 (RF-500TB-14415 engine technical data sheet).

Table 1. Parameters of the motor used in the laboratory model.

Model	Voltage		Power Start		Speed (r/min)	Maximum Efficiency		
	Operation Range	Standard Voltage	Speed (r/min)	Current (A)		Current (A)	Torque (Nm)	Output (W)
RF-500TB-14415	1.5–9.0 V	5.0 V	3100	0.026	2540	0.12	1.23	0.33

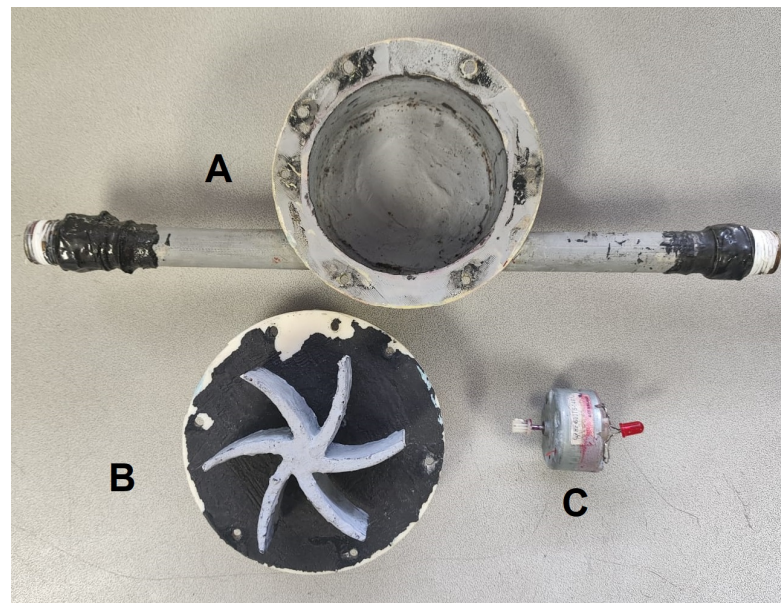


Figure 2. Turbine and casing used in the experiment.

To measure the voltage generated, a mp-9604 Bork multimeter was used.

Design, construction, and tests of the condenser: It was decided to follow the methodology of Pérez Sánchez et al. (2019) [26]. A few modifications were needed for our experiment: a 1/4" diameter flexible copper pipe was used instead of a coil, and thus no inner cylinder was used to hold the flexible pipe in its position.

Outer cylinder inner diameter (Di): 0.163 m

Flexible tubing inner diameter (id): 0.005 m

Flexible tubing outside diameter (OD): 0.007 m

Average propeller diameter (Dh): 0.13 m

Tests on the condenser showed that it could condense water vapor. The water temperature decreased to 60 °C after passing through seven turns of the helical coil heat exchangers. The temperature consistently decreased in all instances, dropping from 96 °C at the turbine outlet to approximately 60 °C at the condenser outlet.

In Figure 3, the components of the laboratory model are labelled, along with the voltmeter used to measure the voltage generated, and the Canon t8i camera used to record the laboratory tests.

The experiment began with the ignition of the heater-evaporator, and it took about 40 min to heat up and reach a vapor pressure of 2.5 psi. At this pressure, the ball valve was opened to 1/3 of its capacity, allowing the turbine to be activated and voltage to be generated. During the experiment, this voltage was recorded at time intervals, ranging from 5 to 15 min.

Due to the sensitivity of the turbine, only one test could be conducted per day. Occasionally, errors occurred when manipulating the ball valve, causing the vapor pressure to decrease more rapidly than desired. In these cases, the generation decreased steadily without achieving equilibrium. When the test was successful, a decrease in generation was observed until the vapor pressure stabilized, remaining constant at that point.

Once the ball valve opening was at precisely 1/3, the power generation achieved equilibrium, and from that point on remained stable for the rest of the experiment. In these cases, the test was considered successful.

After the experimental phase, we validated our numerical model based on the results obtained. This included mesh generation, obtaining residuals and convergence of the model, comparison with laboratory data, replication of the simulation using the working fluid selected, and comparisons of hydrodynamic and thermodynamic behaviors.

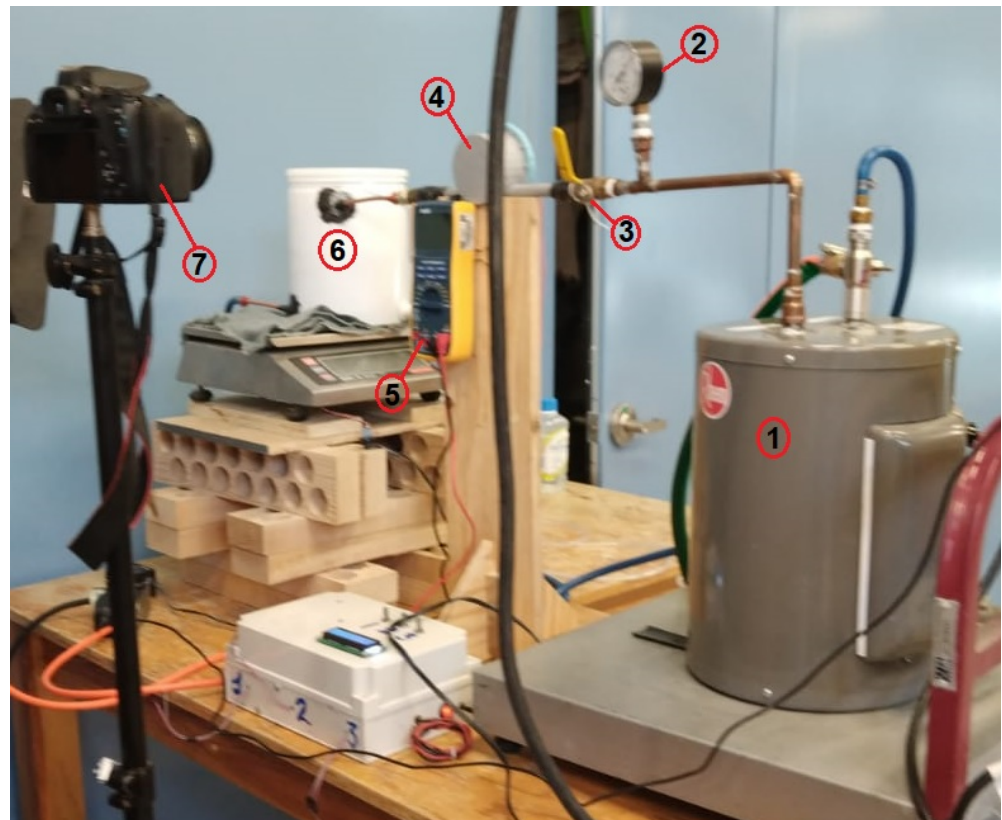


Figure 3. Laboratory set up for steam (1, evaporator; 2, pressure gauge; 3, ball valve; 4, turbine; 5, voltmeter; 6, condenser; 7, camera).

2.3. CFD Modeling

Numerical modeling was used to explore how the axial turbine behaved with different working fluids.

Firstly, the geometric representation of the turbine was defined within the computational domain, forming the foundation for the numerical analysis. Then, the physical properties of the working fluids, as density, viscosity, and thermal conductivity, were specified. Boundary conditions were established to replicate real-world scenarios, and a turbulence model ($k-\varepsilon$) was selected to capture the complexities of the fluid flow.

OpenFOAM was used to carry out the simulations. This is an open-source computational fluid dynamics (CFD) software written in C++. This CFD software solves the Navier–Stokes equations numerically by discretizing the domain in space and time, generating an algebraic system of equations. For the case of compressible fluids, the three-dimensional Favre averaged compressible Navier–Stokes equations are solved. The mass, momentum, and energy conservation equations [27] for a rotating reference frame are as follows:

$$\frac{\partial \rho}{\partial t} = \nabla \cdot (\rho u_{rel}) = 0 \quad (6)$$

$$\frac{\partial (\rho u)}{\partial t} + \nabla \cdot (\rho u_{rel} u) + \rho (w \times u) = -\nabla p + \nabla \cdot \tau \quad (7)$$

$$\frac{\partial (\rho h)}{\partial t} + \nabla \cdot (\rho u_{rel} h) = \frac{Dp}{Dt} + \Omega + \nabla \cdot (k_{eff} \nabla T) \quad (8)$$

where ρ denotes the density, p the pressure, h the enthalpy, τ the shear stress tensor, Ω the dissipation function, and u the absolute velocity, which can be transformed into the relative velocity u_{rel} with respect to the rotating frame of reference by:

$$u_{rel} = u - w \times r \quad (9)$$

With the prescribed angular velocity ω and the effective thermal conductivity k_{eff} .

The rhoPimpleFoam module was used for the simulation of the compressible fluid. The name “rhoPimpleFoam” comes from the combination of two numerical techniques: the PISO method (pressure-implicit with splitting of operators) and the SIMPLE method (semi-implicit method for pressure-linked equations). The PIMPLE method is a variant that combines aspects of both methods, and is especially useful for transient and compressible flows.

2.3.1. Boundary Conditions

The temperature, pressure, and power obtained in the test with steam were used for the numerical simulations. To compare their energy production and thermodynamic behavior, simulations using R134a and ammonia were also performed.

To facilitate the simulations and compare the behavior of the three fluids, certain assumptions were made; the angular frequency of rotation ($\omega = 250$ rad/s) remained constant across the simulations. The thermodynamic and fluid velocities were allowed to vary to achieve equilibrium in accordance with the Bernoulli principle (see Table 2). Consequently, Reynolds numbers were assigned for each simulation: laminar flow conditions were considered for steam modeling, while turbulent flows were assumed for R134a and ammonia, based on the velocity of operation for each case and the calculation of the Reynolds number.

Table 2. Boundary conditions at the inlet of the casing of the simulations.

Fluid	Molecular Weight (M) g/mol	Temp. inlet, to Turbine (T) °C	Inlet Pressure (p) kPa	Inlet Velocity (V)m/s	Mass Flow (\dot{m}) (kg/s)	Reynolds (Re)
Water	18.015	98	93	47	0.00132	16,978.56
Ammonia	17.03	25	550	22	0.00132	96,807.09
R134a	102	20	450	19	0.00132	281,629.57

The inlet boundary conditions (pressure (P), temperature (T), mass rate (\dot{m}), and Reynolds number (Re)) are detailed in Table 2. This also provides information on the thermodynamic properties of the fluid corresponding to the pressure and temperature conditions outlined in Table 3.

Table 3. Thermodynamic properties of fluids for simulation cases.

Fluid	Molecular Weight (M) g/mol	Specific Heat (Cp) kJ/kg*K	Dynamic Viscosity (μ) μ Pa-s	Thermal Conduct. (K) W/mK	Density (ρ) kg/m ³	Prandtl Number	Kinematic Viscosity (ν) m ² /s
Water	18.015	2.0685	12.2	0.0245	0.5509	1.030	2.215×10^{-5}
Ammonia	17.03	2.7726	9.93	0.0269	5.4619	1.023	1.818×10^{-6}
R134a	102	0.9485	11.50	0.0137	21.3075	0.794	5.397×10^{-7}

In the modeling process, it was observed that destabilization of the model occurred at high pressures (>700 kPa). Thus, it was decided to work with a pressure of less than 550 kPa for ammonia, to compare the results with those of steam.

The geometric dimensions used in the numerical model were the same as those of the laboratory model. This choice facilitated a direct comparison of the results obtained with steam, and enabled further analysis with R134a and ammonia.

The power generated was calculated applying Equation (10) and using the efficiency of the small motor used in the laboratory, where τ is the torque, ω is the frequency of rotation (250 rad/s), and η is the efficiency of the small motor used, about 52%.

$$P[W] = \tau \times \omega \times \eta \quad (10)$$

Torque (τ) is calculated per the below equation, where r is the distance from the axis of rotation to the point where the force is applied (this is the lever arm or moment arm):

$$\tau[N - m] = F_T \times r \times \sin(\theta) \quad (11)$$

Finally, the voltage obtained in the laboratory model was compared with the following equation, where A is the amperage of the motor, given by Table 1:

$$V[\text{volts}] = P/A \quad (12)$$

2.3.2. Mesh and Residuals

A mesh was created using the snappyHexMesh module, with the ratio of the spacing in X equal to the spacing in Y , thus achieving better convergence in the calculation, considering the Courant number as approximately equal to 1.

Figure 4 shows the 3D mesh of the casing and turbine with the laboratory dimensions. Figure 5 shows a section of the mesh. The discretization carried out inside the casing and the refinement carried out on the edges of the turbine are visible. From this, the fluid-structure interaction inside the casing was evaluated.

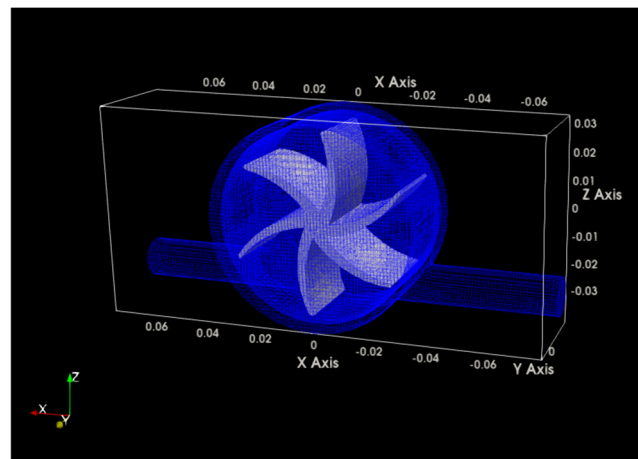


Figure 4. 3D mesh of the axial turbine.

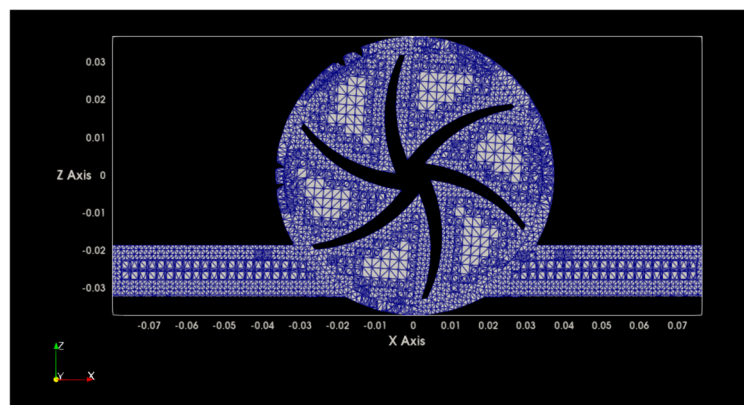


Figure 5. Discretization of the mesh inside the turbine and at the edges of the turbine.

To assess mesh accuracy, residual analyses were conducted. The residuals, serving as indicators of model accuracy, measured the difference between the calculated values and actual values of the variables of interest—velocity, pressure, and temperature—at each point on the grid.

Convergence indicated that the simulation results were consistent and reliable over iterations. The residuals were monitored throughout iterations of the solver and compared

to a set threshold of convergence. When the residuals decreased and remained within the desired threshold, the model was considered to have converged.

For the case of pressure (p), a residual error threshold close to 0.001 was considered, while for velocity (U_x) in the X direction, a residual error threshold close to 0.01 was set.

Figure 5 shows the residuals for the entire simulation, which started at 0 s and ended at 0.05 s. The time range was defined based on the convergence time obtained in the simulations.

Figure 6 shows the convergence of the results for pressure and velocity, starting after 0.02 s and remaining relatively constant until the end of the simulation. In both figures, it can be observed that at the beginning of the simulation, the residuals were greater than the threshold stipulated.

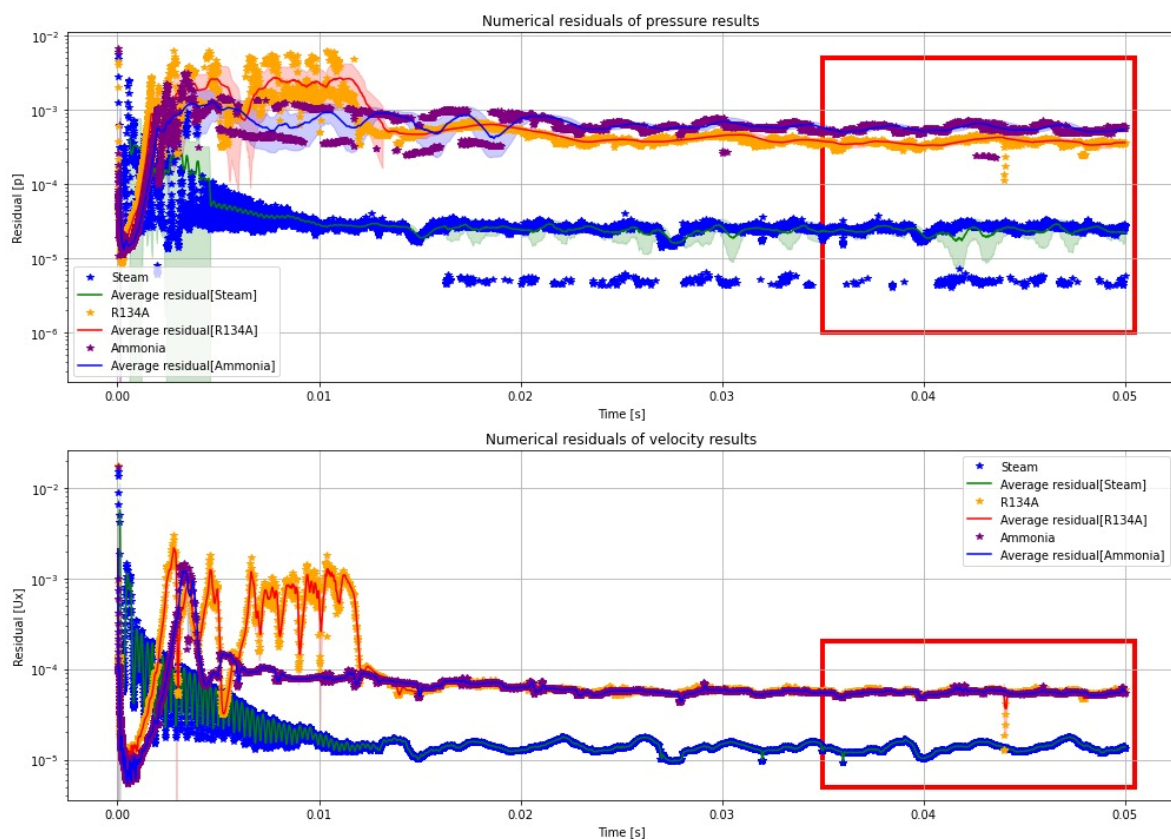


Figure 6. Simulation residuals for the three fluids. The convergence of the variables is highlighted by the red rectangle.

However, at the end of 0.05 s, the residuals converged to less than 0.001 for the pressure field, and 0.01 for the velocity field.

A simulation time of 0.05 s was therefore established to observe the hydrodynamic and thermodynamic behaviors of the three fluids. This period was chosen in an effort to balance computational efficiency and the need to capture the essential transient behavior of the system. This duration proved sufficient to achieve convergence in the key variables.

3. Results

3.1. Selection of the Working Fluid

Based on the analysis of Cerezo et al. (2020), the best working fluids were selected. To make a first filtration, three parameters were considered: the ODP (ozone development potential), the GWP (global warming potential at 100 years), and the boiling pressure at a temperature of 15.56 °C. From the fifty working fluids available in the Engineering Equation Solver (EES) program, a weighting was made. Only six fluids satisfied the parameters established, shown in Table 4.

Table 4. Properties of the fluids included in this study.

Fluids	ODP	GWP	Boiling Pressure at 15.56 °C (kPa)
Ammonia (R717)	0	1	742.5
Isobutane (R600a)	0	20	263.3
Propane (R290)	0	20	742.9
R134a	0	1370	497.5
R152a	0	133	447.1
R407c	0	1700	755.9

The next parameters to be evaluated were flammability, toxicity, parameters for sizing the turbine, and the cost of the working fluids. The flammability and the toxicity were taken from the work of Calm et al. (2011) [28], and are shown in Table 5.

Table 5. Second filtering to evaluate the selection of the working fluid.

Fluids	Flammability	Toxicity	φ	B	Cost \$/kg
Ammonia	16.7	25	10,910.54	15,224,309.10	11.00
Isobutane	1.6	1000	18,849.26	5,193,836.84	248.92
Propane (R290)	2.1	1000	16,321.13	11,505,975.77	325.40
R134a	0	1000	34,352.59	9,443,644.50	157.68
R152a	4.8	1000	25,008.43	8,558,070.76	69.45
R407c	0	1000	31,875.68	12,855,787.83	182.78

Table 6 shows the relevance of the factors to be evaluated. Different considerations were given according to the four different scenarios.

Table 6. Weighting of the aspects to be evaluated.

	Scenario 1	Scenario 2	Scenario 3	Scenario 4
Heating power (GWP)	10	15	25	16.6667
Flammability	15	20	17	16.6667
Toxicity	15	30	17	16.6667
φ	25	10	8	16.6667
B.	25	10	8	16.6667
Approximate costs of the working fluid offered by wholesale suppliers [\$US/kg] subject to market availability.	10	15	25	16.6667

In Scenario 1, emphasis was placed on the size of the plant and safety considerations, prioritizing them over environmental concerns and fluid costs. In Scenario 2, the relevance of safety aspects was highlighted. In Scenario 3, greater significance was assigned to the environmental impact indicators and the costs associated with the working fluid. Scenario 4 assumed equal importance for all criteria.

The results of the linear ponderation of the different scenarios can be seen more easily in Figure 7. As a result of the linear weightings, ammonia and R134a were taken as the most suitable working fluids.

From results obtained using the methodology of Cerezo et al. (2020) [23], six working fluids were identified as feasible for use in a CTEC. Of these, R134a and R407c offered the best results in Scenario 1, as seen in Figure 7. It is worth mentioning that R134a has been used in research related to the organic Rankine cycle (ORC). For instance, in earlier studies conducted by Hsieh et al. [29] and Hijriawan et al. [30], R134a was used in the organic Rankine cycle. Consequently, R134a was chosen as a reference for comparison with ammonia.

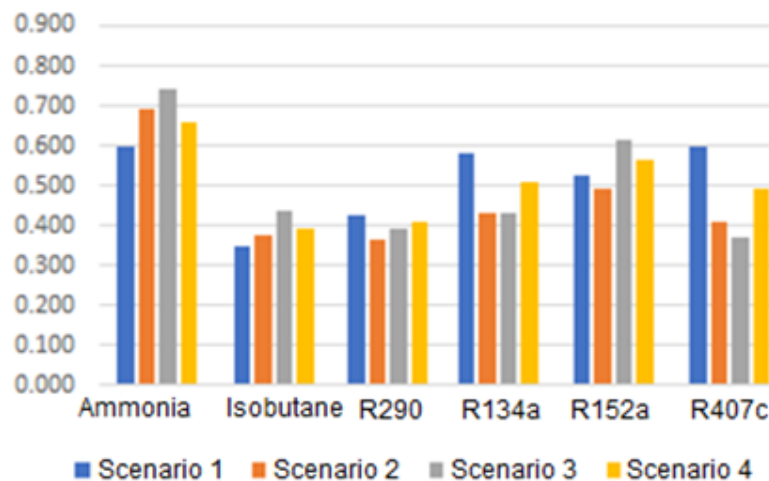


Figure 7. Results of the weightings.

Table 7 shows the thermodynamic properties of the working fluids at the entrance of the turbine. Water is included, as the model was designed to work with steam.

Table 7. Thermodynamic properties of the working fluids to be evaluated at the turbine inlet.

Fluid	Temp. at Turbine Inlet °C	Inlet Pressure KPa	Density kg/m ³
Steam	98	93	0.5509
R134a	20	450	21.051
Ammonia	25	550	4.0204

The results of the laboratory tests were obtained from the digitalization of the data measured during the experiment.

The temperature and pressure values were obtained at each key point. Using the Rankine cycle equations [31], the rest of the values shown in Figure 8 were calculated.

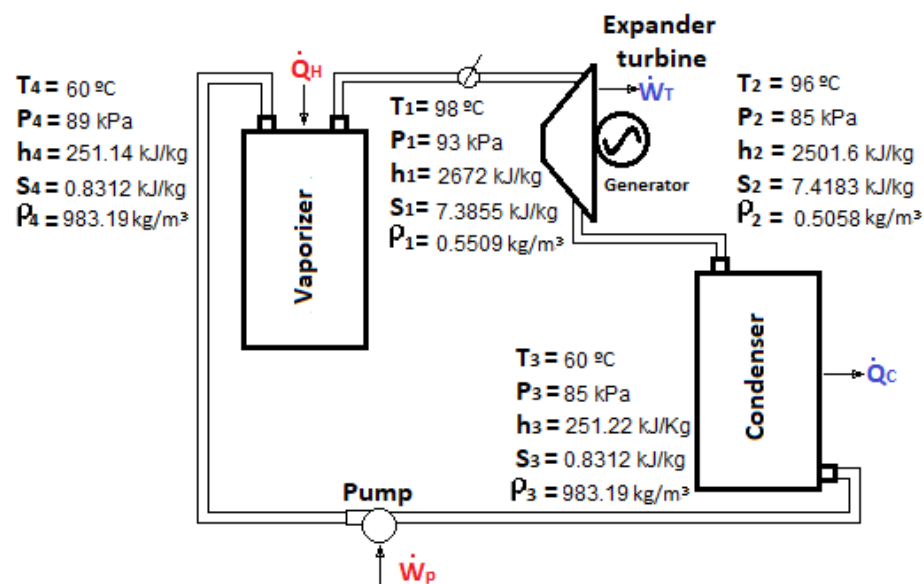


Figure 8. System working with steam, diagram of the Rankine cycle with real data.

Theoretical Rankine cycles were developed using thermodynamic equations [31] incorporating R134a and ammonia (see Figures 9 and 10). These theoretical cycles accounted for specific condensation pressures, with 550 kPa for ammonia and 450 kPa for R134a. It

is important to highlight that reaching these pressures may not be feasible in laboratory experiments, although it is achievable in real plants.

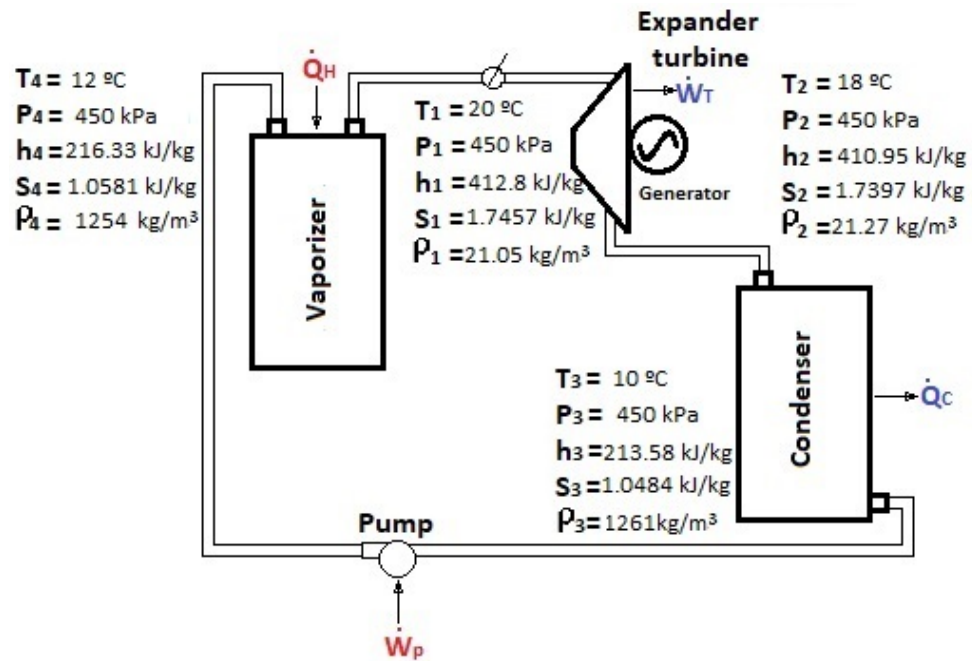


Figure 9. Rankine theoretical cycle using R134a as working fluid.

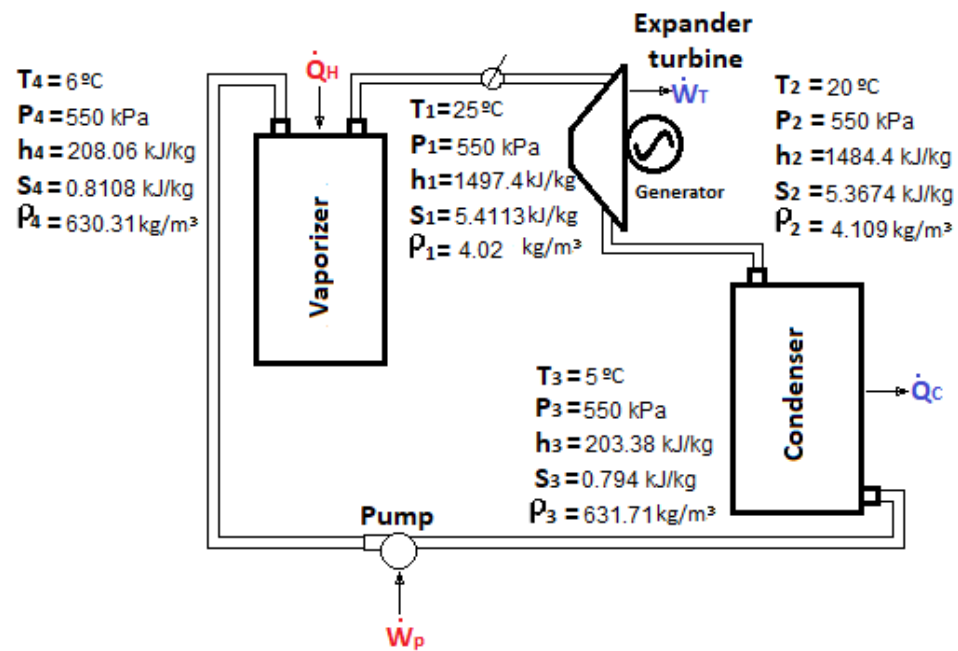


Figure 10. Rankine theoretical cycle using ammonia as working fluid.

Based on the analysis of Figures 8 and 9, and the previous studies of Avery et al. [4], the differences in the cooling relationships of each working fluid can be seen. In the case of R134a, the turbine inlet temperature must be 20 °C, and reduced in the condenser to 10 °C for condensation. For ammonia, these temperature differences were more significant, requiring an inlet temperature of 25 °C for the turbine, and temperatures as low as 5 °C for condensation.

3.2. Experimental Results

Figure 11 shows the voltage achieved in three of the most significant tests. From the beginning of the test, the voltage reached equilibrium until the system stabilized. When the generation remained steady (tests one and three), the test was considered successful.

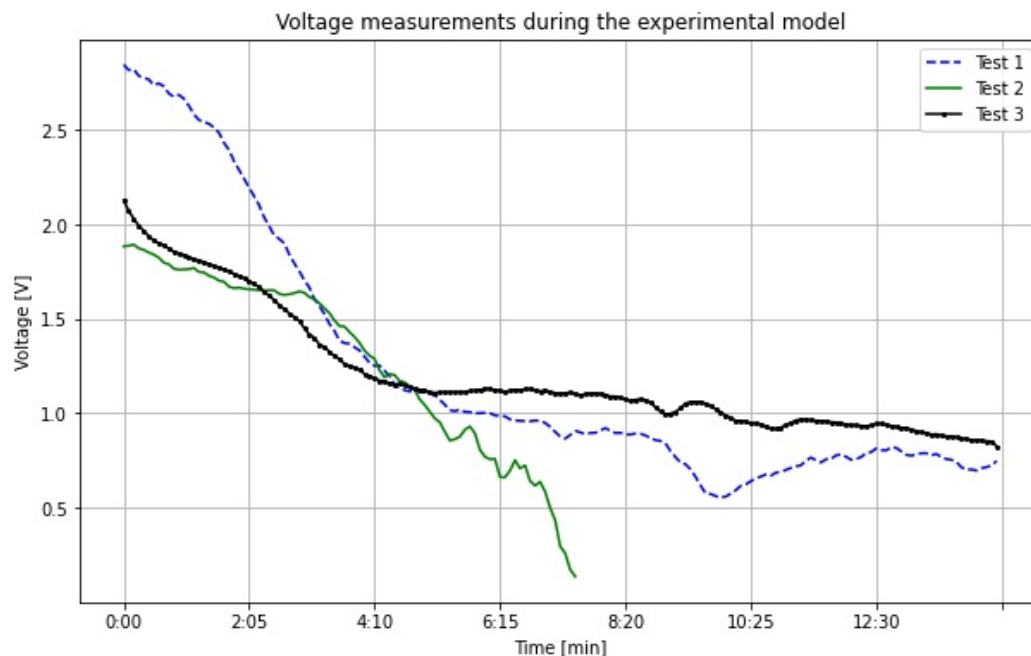


Figure 11. Representative voltage measurements taken in the laboratory test.

In test two, there was a sudden decrease in voltage generated. This was because in the test, the ball valve opened to more than 1/3, causing more vapor pressure to be lost than was being generated. Thus, the generation collapsed, and that test was considered unsuccessful.

During data collection, losses due to leaks in the turbine structure were identified. It was also found that steam generation was not constant over time, as the heater did not maintain a stable power level throughout the duration of the test.

The measurements showed that an average voltage of 1.03 V was obtained between minute 4:10 and minute 14:00 of test three, which was the most stable. This corresponded to a generation of 0.12 W according to the amperage characteristics of the motor (Table 1).

From the insights gained in this phase, calibrating and validating the numerical model followed. The temperature and pressure values used in the laboratory for steam water vapor were used to calibrate the numerical model.

One of the main limitations of this experimentation was the material used to print the 3D turbine. Although results were obtained, only one test was possible per day; if the test lasted longer, structural damage occurred due to the high temperatures involved. The data obtained during the experimental phase demonstrate that electricity generation is possible.

3.3. Numerical Model Results

Results with Steam

This section describes the results of the numerical model using steam and compares them with the results obtained in the laboratory. Based on the simulation results, the forces acting on the turbine were extracted for each time instant, to calculate the torque and the power.

Regarding the pressure and temperature obtained during the simulation, a difference between the inlet and outlet conditions was seen (Table 8 and Figure 12). At the entrance, the temperature was higher, and at the outlet, there was a reduction in temperature and pressure, in line with expectations. As the fluid passed through the turbine and performed work, its temperature and pressure decreased. This was a result of the conversion of thermal

energy into mechanical energy. This study ignored these effects, but further research could focus on optimizing the inlet temperature to enhance overall system efficiency, particularly in the condenser. Calibrating the appropriate temperature at the specified inlet for the condenser may contribute to improvements in the conversion process and overall energy output.

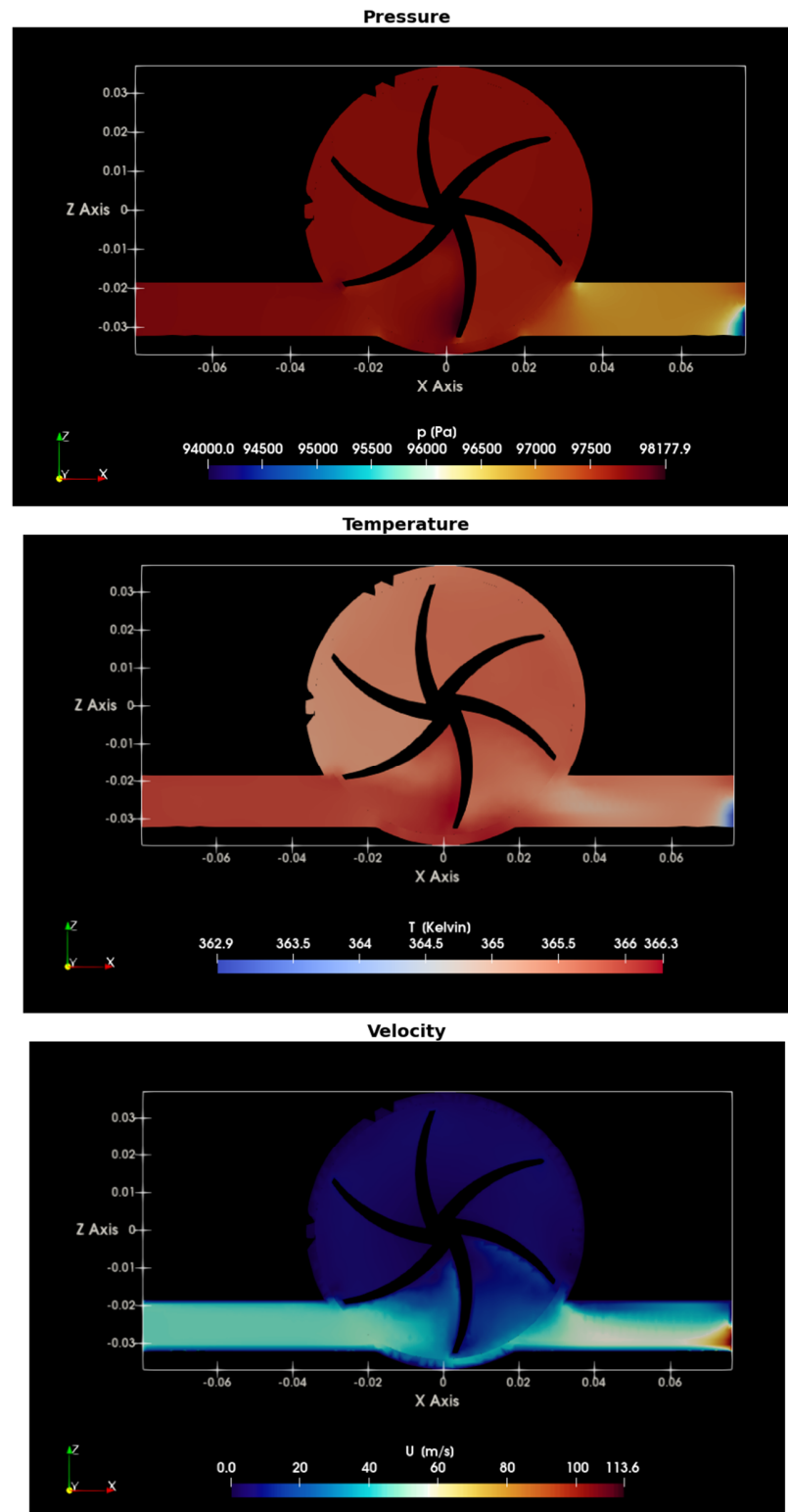
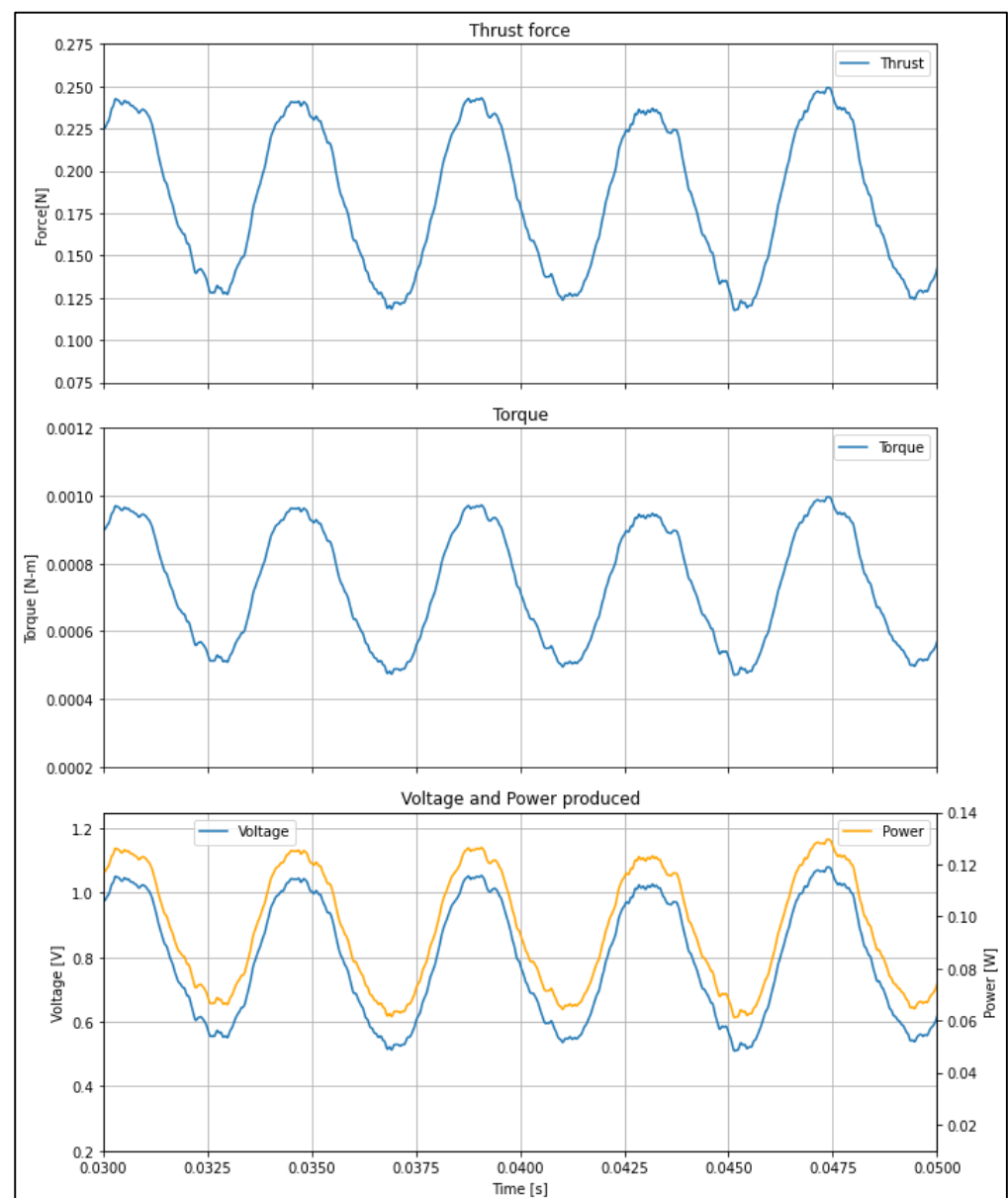


Figure 12. Pressure, temperature, and velocity for steam modelling.

Table 8. Inlet and outlet results.

Fluid	Velocity [m/s]		Pressure [Pa]		Temperature [K]	
	Inlet	Outlet	Inlet	Outlet	Inlet	Outlet
Steam	45.4414	49.900	97,801.6	96,893.2	365.983	365.32
R134a	17.5242	20.240	441,821	441,244	292.986	314.00
Ammonia	18.6888	18.109	541,983	541,538	297.968	326.72

Figure 13 shows the results of pressure, speed, and temperature. It shows the force, torque, and power obtained for the simulation case with steam, with a maximum force of 0.24 N, which resulted in a torque of 0.001 Nm, with an approximate power of 0.13 W considering a motor efficiency of $\eta = 0.52$. Finally, the voltage was obtained using Equations (10)–(12). The results of 0.6 to 1 V coincided closely with previously recorded experimental data (Figure 13).

**Figure 13.** Force, torque, power, and voltage.

The modeled results closely aligned with the laboratory findings in pressure and temperature, showcasing a positive correlation between the theoretical simulation and real-world observations.

3.4. Results with Working Fluids

Using the methodology established in previous stages, simulations were carried out modifying the thermodynamic properties of the R134a and ammonia.

As mentioned earlier, the angular rotation speed for these simulations was 250 rad/s to facilitate comparison with the results obtained with steam.

Therefore, flow inlet velocity was modified for each case (see Table 2) to make a meaningful comparison in an equitable context, in accordance with Bernoulli's principle.

Based on the inlet conditions shown in Table 2, the temperature and pressure for R134a were 450 kPa and 20 °C, and for ammonia 550 kPa and 25 °C, respectively.

Figure 14 shows both configurations at the turbine inlet, including the lower pressure at the turbine outlet, mentioned earlier. In the figure, the comparable dynamic and thermodynamic behavior of the two fluids is noticeable. This is crucial for comparing the thrust and power produced by each fluid.

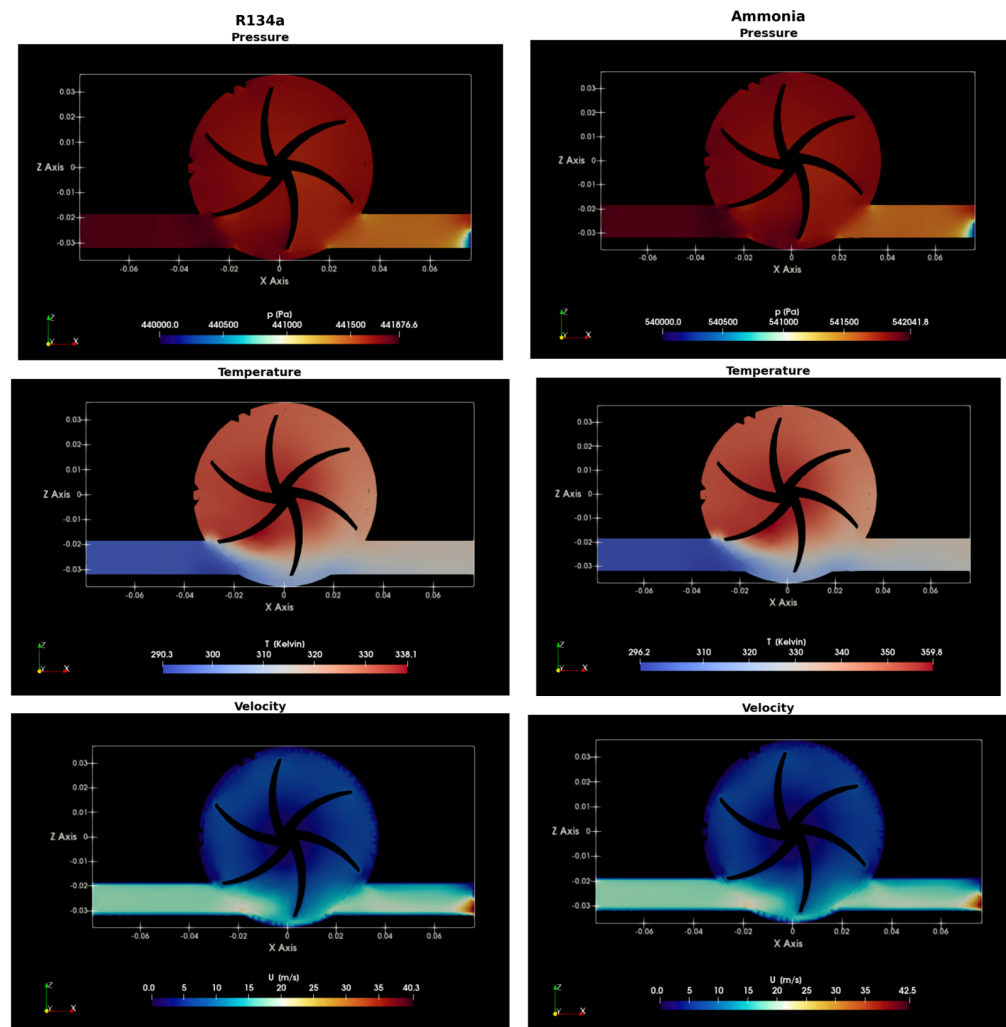


Figure 14. Pressure, temperature, and velocity results for R134a and ammonia.

Table 8 presents the simulation results using R134a and ammonia as working fluids, and the pressure, temperature, and velocity values for each. The analysis involved extracting forces to determine torque and power.

A small inconsistency was noted at the casing outlet, causing a rise in both velocity and temperature, as detailed in Table 8. This was probably due to the insufficient length of the pipe. The unexpected temperature increase contrasted with the expected decrease calculated for the Rankine cycle. This inconsistency highlights the need for more in-depth investigation into the simulation parameters and conditions to better understand these deviations.

Table 9 and Figure 15 illustrate the results for the forces obtained in each case of this study, showing the force acting on the turbine, as well as the corresponding torque and power produced. It is important to mention that the figure also highlights the maximum values of power and torque, and provides insights into the peak performance achieved in each scenario, which are quite similar. Although the R134a and ammonia fluids differed in key properties, such as density and thermodynamic properties, the fact that they generated comparable forces suggests that both are capable of similar work in the turbine.

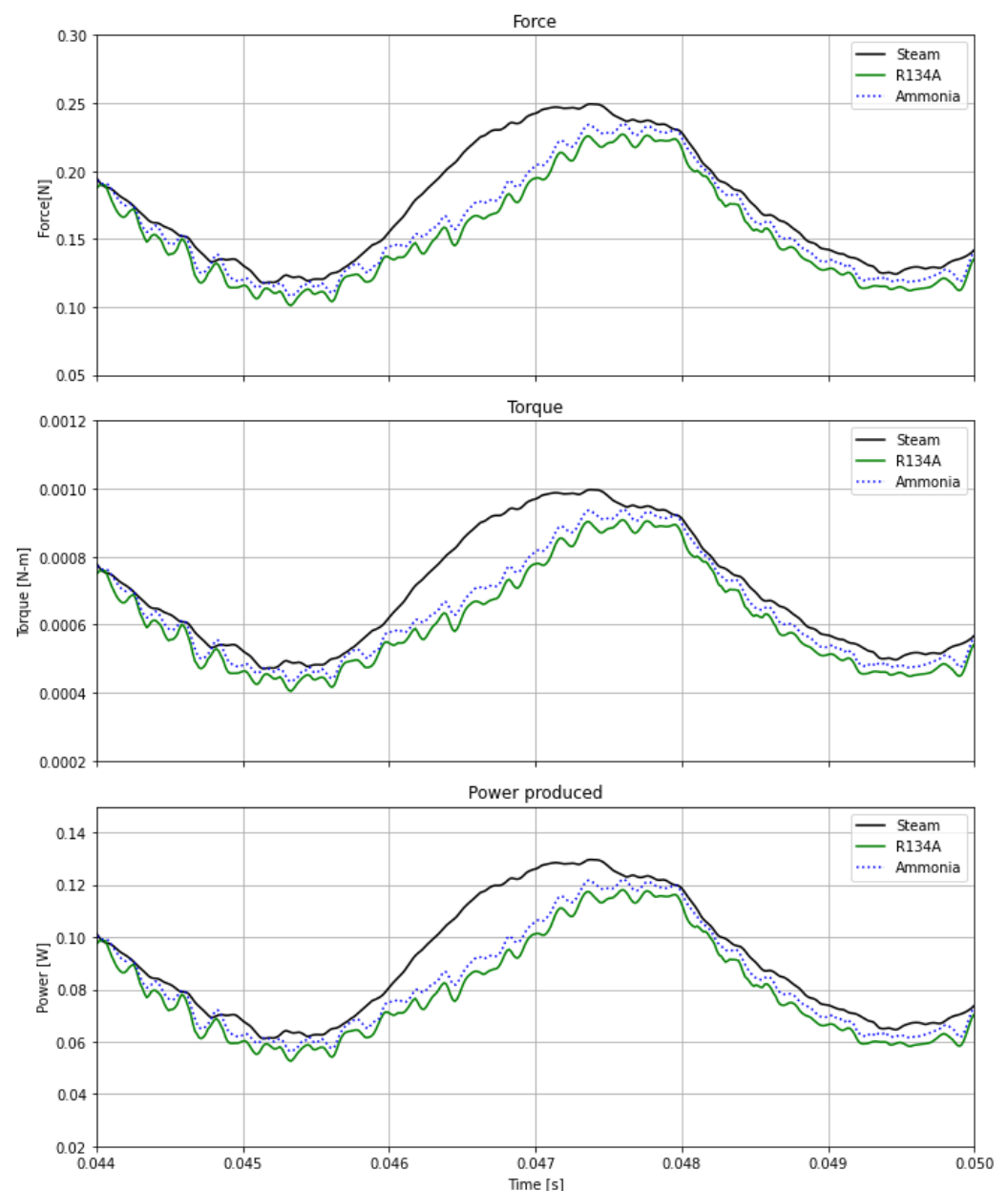


Figure 15. Steam, R134a, and ammonia.

Table 9. Thrust, torque, and power results.

Fluids	Thrust [N]	Torque [N-m]	Power [W]
Steam	0.2493	0.00100	0.1296
R134a	0.2270	0.00091	0.1181
Ammonia	0.2348	0.00094	0.1221

The results demonstrated a strong agreement with the experimental findings from the second and third steam tests, with both sets of data yielding similar voltage values under the given pressure and temperature conditions. The accuracy of the voltage results obtained from the numerical model, which registered a maximum of 1.08 V, compared to the experimental results, with a mean voltage of 0.8333 V, was approximately 77.55%. This discrepancy can likely be attributed to fluctuations in pressure experienced during the experiment, leading to variations in the measured voltage.

The extension of the numerical scheme to simulate R134a and ammonia could yield valuable insights, as these results demonstrated similar values of thrust and power, attributed to the proximity of their physical and thermodynamic properties. However, it is crucial to note that further analysis is warranted to assess the feasibility of operating under high-pressure conditions, particularly for ammonia. It was observed that the computational fluid dynamics (CFD) simulations faced limitations in accurately capturing these conditions for ammonia. Therefore, additional investigations are necessary to determine the suitability of the numerical scheme for such scenarios.

4. Conclusions

The overall results suggest that to generate energy from a CTEC, the working fluid R134a is a more efficient and promising option than ammonia, which is more commonly used.

The corresponding theoretical cycles for R134a and ammonia were determined. For ammonia, the cold temperatures needed for condensation are found deeper in the thermocline of the sea. This implies that greater pumping power would be required to extract the cold water for the condenser, meaning that more energy would be needed, as the water would have to come from deeper in the sea.

A laboratory model was constructed to collect data on the performance of the turbine with steam as the working fluid. The results obtained were then compared, and the numerical model adjusted accordingly.

The results of the numerical modeling showed that the working fluids R134a and ammonia were suitable for CTEC energy production. However, ammonia requires substantially higher pressures and higher condensation temperatures, which implies a significant increase in energy load for its efficient operation.

The rhoPimpleFoam module in OpenFOAM effectively modeled the thermodynamic properties, pressures, and fluid velocities of steam and R134a. However, instabilities arose in high-pressure situations, requiring future research to adjust the underlying code.

A minor inconsistency at the casing outlet, showing increased velocity and temperature, indicated the need for further investigation into simulation parameters, conditions, and pipe dimensions.

Author Contributions: Conceptualization, A.A., R.S. and E.M.; methodology, A.A. and E.M.; software, A.A. and L.D.L.; validation, A.A. and L.D.L.; formal analysis, A.A. and E.M.; investigation, A.A.; resources, E.M. and R.S.; writing—review and editing A.A., L.D.L., E.M. and R.S.; supervision, E.M.; project administration, A.A. and E.M.; funding acquisition, E.M. and R.S. All authors have read and agreed to the published version of the manuscript.

Funding: This research was funded by CEMIE-Océano (Mexican Centre for Innovation in Ocean Energy), financed by CONACYT-SENER-Sustentabilidad Energética.

Data Availability Statement: Data are available upon request.

Acknowledgments: We would like to thank all of the laboratory staff who collaborated on the construction and experimentation of the laboratory model. Aliet Achkienasi Amezcua thanks CONAH-CYT for the doctoral fellowship (CVU: 518490726).

Conflicts of Interest: The authors declare no conflicts of interest.

Nomenclature

OTEC	Ocean Thermal Energy Converter
CTEC	Coastal Thermal Energy Converter
CFD	Computational Fluid Dynamics
W	Watts
kW	Kilo Watts
MW	Mega Watts
ORC	Organic Rankine Cycle
ODP	Ozone layer destruction potential
GWP	Global Warming Potential
B	Sizing parameter
ΔH_{lg}	Enthalpy change due to phase change
p_v	Saturation pressure at 1 atm in kPa
M	Molecular weight (g/mol)
C_p	Specific heat
a	Exchanger area (m ²)
\dot{Q}	Heat flux
U_0	Global coefficient of the exchanger
k	Thermal conductivity
ρ_l	Density (kg/m ³)
θ	Pipe diameter (m)
μ_l	Dynamic viscosity (Pa s)
p	Pressure
h	enthalpy
τ	shear stress tensor
Ω	dissipation function
u	absolute velocity
u_{rel}	relative velocity
ω	angular velocity
k_{eff}	effective thermal conductivity
Re	Reynolds number
\dot{m}	Mase rate

References

1. Elavarasan, R.M. The motivation for renewable energy and its comparison with other energy sources: A review. *Eur. J. Sustain. Dev. Res.* **2019**, *3*, em0076. [[CrossRef](#)] [[PubMed](#)]
2. Barros, C.P.; Peypoch, N. Technical efficiency of thermoelectric power plants. *Energy Econ.* **2008**, *30*, 3118–3127. [[CrossRef](#)]
3. Garduño-Ruiz, E.P.; Silva, R.; Rodríguez-Cueto, Y.; García-Huante, A.; Olmedo-González, J.; Martínez, M.L.; Wojtarowski, A.; Martell-Dubois, R.; Cerdeira-Estrada, S. Criteria for optimal site selection for ocean thermal energy conversion (Otec) plants in Mexico. *Energies* **2021**, *14*, 2121. [[CrossRef](#)]
4. Avery, W.H.; Wu, C. *Renewable Energy from the Ocean: A Guide to OTEC*; Oxford University Press: Oxford, UK, 1994.
5. Liu, W.; Xu, X.; Chen, F.; Liu, Y.; Li, S.; Liu, L.; Chen, Y. A review of research on the closed thermodynamic cycles of ocean thermal energy conversion. *Renew. Sustain. Energy Rev.* **2020**, *119*, 109581. [[CrossRef](#)]
6. Cohen, R. Energy from the ocean. *Philosophical Transactions of the Royal Society of London. Ser. A Math. Phys. Sci.* **1982**, *307*, 405–437.
7. Mitsui, T.; Ito, F.; Seya, Y.; Nakamoto, Y. Outline of the 100 kw Otec Pilot Plant in the Republic of Naure. *IEEE Trans. Onpower Appar. Syst.* **1983**, *PAS-102*, 3167–3171. [[CrossRef](#)]
8. Vega, L.A. Ocean thermal energy conversion primer. *Mar. Technol. Soc. J.* **2002**, *36*, 25–35. [[CrossRef](#)]
9. Academy, I.N.S. *Pursuit and Promotion of Science: The Indian Experience*; Indian National Science Academy: New Delhi, India, 2001.
10. Rajagopalan, K.; Nihous, G.C. Estimates of global Ocean Thermal Energy Conversion (OTEC) resources using an ocean general circulation model. *Renew. Energy* **2013**, *50*, 532–540. [[CrossRef](#)]

11. Vyawahare, M.; Climatewire. Hawaii First to Harness Deep-Ocean Temperatures for Power. Available online: <https://www.scientificamerican.com/article/hawaii-first-to-harness-deep-ocean-temperatures-for-power/> (accessed on 5 April 2024).
12. Zhang, C.; Wu, Z.; Wang, J.; Ding, C.; Gao, T.; Chen, Y. Thermodynamic performance of a radial-inflow turbine for ocean thermal energy conversion using ammonia. *Renew. Energy* **2023**, *202*, 907–920. [[CrossRef](#)]
13. Ma, Q.; Gao, Z.; Huang, J.; Mahian, O.; Feng, X.; Lu, H.; Wang, S.; Wang, C.; Tang, R.; Li, J. Thermodynamic analysis and turbine design of a 100 kW OTEC-ORC with binary non-azeotropic working fluid. *Energy* **2023**, *263*, 126097. [[CrossRef](#)]
14. Yang, M.H.; Yeh, R.H. Investigation of the potential of R717 blends as working fluids in the organic Rankine cycle (ORC) for ocean thermal energy conversion (OTEC). *Energy* **2022**, *245*, 123317. [[CrossRef](#)]
15. Zheng, G.; Xu, P.; Li, L.; Fan, X. Investigations of the Formation Mechanism and Pressure Pulsation Characteristics of Pipeline Gas-Liquid Slug Flows. *J. Mar. Sci. Eng.* **2024**, *12*, 590. [[CrossRef](#)]
16. Yan, Q.; Li, D.; Wang, K.; Zheng, G. Study on the Hydrodynamic Evolution Mechanism and Drift Flow Patterns of Pipeline Gas-Liquid Flow. *Processes* **2024**, *12*, 695. [[CrossRef](#)]
17. da Silva, E.R.; Kyprianidis, K.G.; Camacho, R.G.R.; Säterskog, M.; Angulo, T.M.A. Preliminary design, optimization and CFD analysis of an organic rankine cycle radial turbine rotor. *Appl. Therm. Eng.* **2021**, *195*, 117103. [[CrossRef](#)]
18. Yu, Z.; Wang, C.; Rong, F.; Liang, W. Optimal coupling design for organic Rankine cycle and radial turbine rotor using CFD modeling, machine learning and genetic algorithm. *Energy Convers. Manag.* **2023**, *275*, 116493. [[CrossRef](#)]
19. Obert, B.; Cinnella, P. Comparison of steady and unsteady RANS CFD simulation of a supersonic ORC turbine. *Energy Procedia* **2017**, *129*, 1063–1070. [[CrossRef](#)]
20. Jayakumar, J.; Mahajani, S.; Mandal, J.; Vijayan, P.; Bhoi, R. Experimental and CFD estimation of heat transfer in helically coiled heat exchangers. *Chem. Eng. Res. Des.* **2008**, *86*, 221–232. [[CrossRef](#)]
21. Deng, R.; Xie, L.; Lin, H.; Liu, J.; Han, W. Integration of thermal energy and seawater desalination. *Energy* **2010**, *35*, 4368–4374. [[CrossRef](#)]
22. Yoon, J.I.; Son, C.H.; Baek, S.M.; Kim, H.J.; Lee, H.S. Efficiency comparison of subcritical OTEC power cycle using various working fluids. *Heat Mass Transf.* **2014**, *50*, 985–996. [[CrossRef](#)]
23. Cerezo-Acevedo, E.; Cupul, J.G.T.; Medina, V.M.R.; Barragan, E.G.; Mendieta, M.A. *Analysis and Development of Closed Cycle OTEC System*; IntechOpen: London, UK, 2020.
24. Domanski, P. Evolution of Refrigerant Application. In Proceedings of the International Congress on Refrigeration, Milano, IT, Italy, 4 May 1999; Available online: https://tsapps.nist.gov/publication/get_pdf.cfm?pub_id=860786 (accessed on 18 April 2024).
25. European Parliament; Council of the European Union. Regulation (EU) No 517/2014 of the European Parliament and of the Council of 16 April 2014 on Fluorinated Greenhouse Gases and Repealing Regulation (EC) No 842/2006: Text with EEA Relevance. Official Journal of the European Union, L 150/195. 2014. Available online: <https://eur-lex.europa.eu/legal-content/EN/TXT/?uri=celex:32014R0517> (accessed on 15 February 2024).
26. Pérez Sánchez, A.; Pérez Sánchez, E.; Heredia Sánchez, A.; Pazos Amayuela, L. Diseño de un intercambiador de calor de serpentín para el enfriamiento de acetona. *Nexo Rev. Científica* **2019**, *32*, 61–74. [[CrossRef](#)]
27. Heinrich, M.; Schwarze, R. Simulation and validation of the compressor stage of a turbocharger using openfoam. In Proceedings of the 8th Institution of Mechanical Engineers–8th International Conference on Compressors and Their Systems, London, UK, 9–10 September 2013; pp. 659–667.
28. Calm, J.M.; Hourahan, G.C. Physical, safety, and environmental data for current and alternative refrigerants. In Proceedings of the 23rd International Congress of Refrigeration (ICR2011), Prague, Czech Republic, 21–26 August 2011; pp. 21–26.
29. Hsieh, J.C.; Chen, Y.H.; Hsieh, Y.C. Experimental study of an organic Rankine cycle with a variable-rotational-speed scroll expander at various heat source temperatures. *Energy* **2023**, *270*, 126956. [[CrossRef](#)]
30. Hijriawan, M.; Pambudi, N.A.; Wijayanto, D.S.; Biddinika, M.K.; Saw, L.H. Experimental analysis of R134a working fluid on Organic Rankine Cycle (ORC) systems with scroll-expander. *Eng. Sci. Technol. Int. J.* **2022**, *29*, 101036. [[CrossRef](#)]
31. Cengel, Y.A.; Boles, M.A.; Kanoglu, M. *Thermodynamics: An Engineering Approach*; McGraw-Hill: New York, NY, USA, 2011; Volume 5.

Disclaimer/Publisher's Note: The statements, opinions and data contained in all publications are solely those of the individual author(s) and contributor(s) and not of MDPI and/or the editor(s). MDPI and/or the editor(s) disclaim responsibility for any injury to people or property resulting from any ideas, methods, instructions or products referred to in the content.